Epithelial Na$^+$ Channel Subunit Stoichiometry

Alexander Staruschenko,* Emily Adams,* Rachell E. Booth,[†] and James D. Stockand*

*Department of Physiology, University of Texas Health Science Center at San Antonio, San Antonio, Texas; and [†]Department of Chemistry and Biochemistry, Texas State University, San Marcos, Texas

ABSTRACT   Ion channels, including the epithelial Na$^+$ channel (ENaC), are intrinsic membrane proteins comprised of component subunits. Proper subunit assembly and stoichiometry are essential for normal physiological function of the channel protein. ENaC comprises three subunits, α, β, and γ, that have common tertiary structures and much amino acid sequence identity. For maximal ENaC activity, each subunit is required. The subunit stoichiometry of functional ENaC within the membrane remains uncertain. We combined a biophysical approach, fluorescence intensity ratio analysis, used to assess relative subunit stoichiometry with total internal reflection fluorescence microscopy, which enables isolation of plasma membrane fluorescence signals, to determine the limiting subunit stoichiometry of ENaC within the plasma membrane. Our results demonstrate that membrane ENaC contains equal numbers of each type of subunit and that at steady state, subunit stoichiometry is fixed. Moreover, we find that when all three ENaC subunits are coexpressed, heteromeric channel formation is favored over homomeric channels. Electrophysiological results testing effects of ENaC subunit dose on channel activity were consistent with total internal reflection fluorescence/fluorescence intensity ratio findings and confirmed preferential formation of heteromeric channels containing equal numbers of each subunit.

INTRODUCTION

The epithelial Na$^+$ channel (ENaC) is an ion channel localized to the luminal plasma membrane of epithelial cells lining hollow organs involved in Na$^+$ homeostasis, such as the distal colon and distal renal nephron (Snyder, 2002; Hummler and Horisberger, 1999). Activity of ENaC is rate limiting for Na$^+$ transport across these epithelia. In addition, ENaC is found in the luminal membrane of specialized epithelia, such as that in the inner ear, responsible for generating and maintaining rare K$^+$ rich extracellular fluid compartments. Moreover, ENaC shares sequence homology and secondary/tertiary structure with neuronal degenerins and acid-sensing ion channels, which play important roles in sensory perception and synaptic transmission. Together these channels comprise the ENaC/Deg gene superfamily (Benos and Stanton, 1999; Kellenberger and Schild, 2002). Importantly, gain and loss of ENaC function and regulation lead to severe blood pressure and electrolyte disorders in humans (Lifton et al., 2001). Abnormal ENaC activity, moreover, is beginning to be recognized as contributing to the disease processes associated with cystic fibrosis and polycystic kidney disease, as well as several other disorders with abnormal epithelial cell transport (Mall et al., 2004; Rohatgi et al., 2003; Veizis et al., 2004).

Similar to most other ion channels, ENaC is a heteromeric protein complex containing several subunits. For maximal activity, the channel must be formed from at least three similar but distinct subunits: α, β, and γ-ENaC (Canessa

et al., 1994; McNicholas and Canessa, 1997; Fyfe and Canessa, 1998). Each of these subunits has two relatively short cytosolic tails separated by a large extracellular loop. Thus, each subunit also has two transmembrane domains. Although it is accepted that each of the three ENaC subunits contributes to formation of the functional channel pore (Firsov et al., 1998; Canessa et al., 1994), the actual subunit stoichiometry of the channel remains uncertain and controversial. In addition, ENaC subunits, in particular α-ENaC, may form homomeric channels with distinct biophysical properties (Canessa et al., 1993). The precision and practice of forming homomeric versus heteromeric channels, though, remains unresolved. A better understanding of the subunit stoichiometry of ENaC and the precision of subunit arrangement is paramount to solving the molecular mechanisms modulating activity of this channel and to understanding how cellular signaling inputs modulate channel openings and closings, as well as membrane localization.

One proposed subunit stoichiometry for ENaC is that the fully oligomerized channel complex within the plasma membrane contains 2α subunits and one each of the β- and γ-subunits. This heterotetrameric structure for ENaC is attractive for it has parallels with the fourfold internal symmetry around a central conducting pore established for several K$^+$ channels, particularly for those channels comprising subunits with only two transmembrane domains, which is a feature shared with ENaC (Firsov et al., 1998; Kosari et al., 1998). In contrast to this molecular architecture, we and others have proposed that ENaC contains several copies of each subunit in a higher order structure (Staruschenko et al., 2004a; Eskandari et al., 1999; Snyder et al., 1998). Experimental support, often arising from similar experimental designs, has been provided for both subunit

stoichiometries (Firsov et al., 1998; Kosari et al., 1998; Snyder et al., 1998; Eskandari et al., 1999). Here, we have determined relative subunit stoichiometry of heteromeric ENaC at the surface membrane using a novel fluorescence-based approach. We have determined the ratio of fluorophore-tagged ENaC subunits within the membrane channel by directly quantifying eCFP and eYFP fluorescence in the surface membrane using total internal reflection fluorescence microscopy. We also have determined the relative subunit stoichiometry in functional ENaC by directly quantifying channel activity in subunit titration experiments. Our results show that functional ENaC within the membrane contains equal numbers of the α-, β-, and γ-subunits. We also find that heteromeric channels are preferentially formed over homomeric channels when all three subunits are coexpressed. The current findings, in consideration of previous findings regarding ENaC subunit stoichiometry, are most consistent with a higher order channel structure.

MATERIALS AND METHODS

Channel constructs and cell culture

CHO and COS-7 cells were maintained with standard culture conditions (DMEM + 10% FBS, 37°C, 5% CO_2) and transfected using the Polyfect reagent (Qiagen, Valencia, CA) as described previously (Staruschenko et al., 2004a,b,c). The plasmids encoding α-, β-, and γ-ENaC, as well as ENaC subunits genetically linked to NH_2-terminal eCFP and eYFP have been described previously (Staruschenko et al., 2004a,b,c). As noted in these earlier publications, channels comprising eCFP- and eYFP-tagged subunits exhibit functional behavior indistinguishable from those without fluorescent tags. Plasmids encoding membrane localized eCFP-m and eYFP-m were from Clontech (Palo Alto, CA). The plasmid encoding CGY-m, which is a membrane localized fusion protein of eCFP and eYFP containing the COOH-terminal Rho sequence RQKKRRGCLLL, was a kind gift from P. Slesinger (Salk Institute for Biological Studies, San Diego, CA).

Total internal reflection fluorescence microscopy

Fluorescence emissions from eCFP- and eYFP-tagged channel subunits were collected using total internal reflection fluorescence (TIRF) (also called evanescent-field) microscopy to selectively illuminate the plasma membrane and thus, focus on signals from membrane ENaC. TIRF generates an evanescent field that declines exponentially with increasing distance from the interface between the coverglass and plasma membrane illuminating only a small optical slice of the cell including the plasma membrane (Taraska et al., 2003; Steyer and Almers, 2001). All TIRF experiments were performed in the total internal reflection fluorescence microscopy core facility housed within the Department of Physiology at the University of Texas Health Science Center, San Antonio (http://physiology.uthscsa.edu/tirf).

We have previously described imaging ENaC channels containing eCFP- and eYFP-tagged subunits with TIRF microscopy (Staruschenko et al., 2004c). The methods used in this study closely followed these published protocols. In brief, fluorescence emissions from fluorophore-tagged ENaC were collected using an inverted TE2000 microscope with through-the-lens TIRF imaging (Nikon, Tokyo, Japan). Samples were viewed through a plain Apo TIRF 60× oil-immersion, high-resolution (1.45 N.A.) objective. Fluorescence from tagged subunits was collected with one of two settings: For Figs. 3–6, an Argon-ion laser with excitation filters of 458 ± 5 and 488 ± 5 nm was used to excite eCFP- and eYFP-tagged subunits, respectively. Emissions from the eCFP and eYFP fluorophores subsequently passed

through 480 ± 15 (465-nm dichroic) and 535 ± 25 nm (505-nm dichroic) single pass filters, respectively. With these settings, there was little bleed-through of the eYFP signal into the CFP field (0.67 ± 0.10% for cells expressing eYFP-m alone, $n = 16$) but, as expected modest bleed-through of the eCFP signal into the YFP field (30 ± 2.0% for cells expressing eCFP-m alone, $n = 16$). Because FIR is a ratiometric approach, bleed-through correction is included in the scaling factor C (see below). Thus, bleed-through primarily affected the current results by increasing background noise. To decrease noise, some experiments were performed using different excitation/emission settings. For Figs. 1, 2, and 9, eCFP and eYFP were excited with a 442-nm Melles Griot dual-pulsed solid state and 514-nm Argon-ion laser, respectively, with an acoustic optic tunable filter used to select excitation wavelengths (Prairie Technology, Middleton, WI). Emissions from eCFP and eYFP passed through an image splitting device (Dual-View, Optical Insights, Tucson, AZ) using a 505-nm dichroic to split emissions, which then passed through 470 ± 15 and 550 ± 25 nm emission filters, respectively. There was no bleed-through with either eYFP and eCFP with these latter settings (see Fig. 1). With both settings, fluorescence images were collected and processed with a charge-coupled device camera interfaced to a PC running Metamorph software.

Fluorescence intensity ratio analysis

Zheng and Zagotta (2004) were the first to describe fluorescence intensity ratio (FIR) analysis. Our FIR analysis closely followed their work with the exception that we collected fluorescence emissions with TIRF microscopy in mammalian cells. For TIRF-FIR experiments, subconfluent COS-7 cells grown on glass bottom 35-mm^2 tissue culture dishes were transfected with either CGY-m, eYPF-m and eCFP-m, or eYFP- and eCFP-tagged ENaC subunit cDNAs (0.2 μg each per dish). Subunits were expressed where one subunit was tagged with eCFP, another tagged with eYFP, and the third distinct subunit not tagged (e.g., eCFP-αENaC + eYFP-βENaC + γENaC). To facilitate ratiometric analysis, we coexpressed in a parallel set of cells tagged subunits with the fluorophores exchanged (i.e., eCFP-βENaC + eYFP-αENaC + γENaC). In some cases, cells expressing one type of eCFP-tagged subunit plus the two other distinct subunits eYFP-tagged (i.e., eCFP-αENaC + eYFP-βENaC + eYFP-γENaC) and its parallel with exchanged fluorophores (i.e., eYFP-αENaC + eCFP-βENaC + eCFP-γENaC) were used.

The covalent linkage between the fluorophore and tagged ENaC subunit ensured that the intensity of fluorescence observed in TIRF was proportional to the number of subunits of that type in the plasma membrane. When eCFP-tagged X-subunits and eYFP-tagged Y-subunits are coexpressed, the intensities of eCFP and eYFP can then be calculated as:

$$F_{eCFP} = C_1[X] \tag{1}$$
$$F_{eYFP} = C_2[Y], \tag{2}$$

where F_{eCFP} and F_{eYFP} are eCFP and eYFP intensities with excitation of 458 (or 442) and 488 (or 514) nm, respectively. $[X]$ and $[Y]$ are the number of the X-eCFP and Y-eYFP subunits; and C_1 and C_2 are constants reflecting laser intensities, system transfer function, bleed-through, properties of the fluorophores, etc. The fluorescence intensity ratio then is defined as:

$$k_1 = F_{eCFP}/F_{eYFP} = (C_1[X])/(C_2[Y]) = C \times ([X]/[Y]), \tag{3}$$

where the constant C is a correction factor equal to C_1/C_2.

Similarly, FIR from the parallel set of cells expressing tagged subunits with exchanged fluorophore combinations of X-eYFP and Y-eCFP subunits is:

$$k_2 = F_{eCFP}/F_{eYFP} = C/([X]/[Y]), \tag{4}$$

and from Eqs. 3 and 4, both the subunit ratio and constant C can be determined such that:
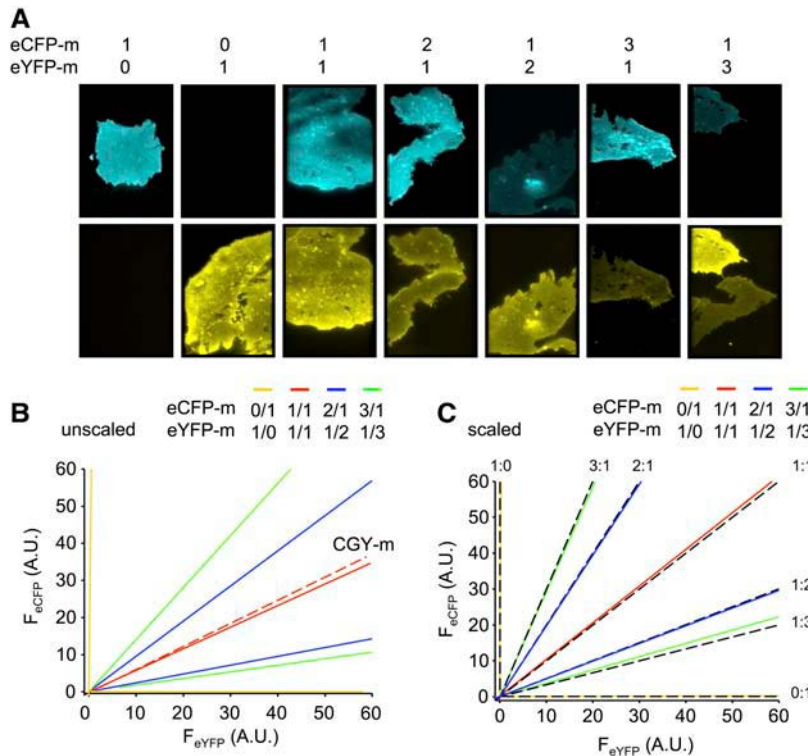
A

FIGURE 1 FIR-TIRF controls. (*A*) Fluorescence micrographs showing the plasma membrane of COS-7 cells expressing eCFP-m and eYFP-m at cDNA ratios of 1:0, 0:1, 1:1, 2:1, 1:2, 3:1, and 1:3 with the top and bottom rows showing eCFP (*pseudocolored cyan*) and eYFP (*pseudocolored yellow*) emissions, respectively. Cells were imaged with TIRF microscopy. (*B*) Unscaled best-fit linear regression lines of data points for eCFP and eYFP emissions from cells expressing eCFP-m and eYFP-m at cDNA ratios of 1:0 and 0:1 (*yellow*); 1:1 (*red*); 2:1 and 1:2 (*blue*); and 3:1 and 1:3 (*green*). Also shown is the (*dashed red*) regression line for eCFP and eYFP emissions from cells expressing the CGY-m fusion protein, which contains the fluorophores as a FRET pair. (*C*) Results from panel *B* scaled using the constant *C*. Black dashed lines predict eCFP-m and eYFP-m membrane levels at the indicated expression ratios.

$$[X]/[Y] = \sqrt{(k_1/k_2)}, \tag{5}$$

and

$$C = \sqrt{(k_1 \times k_2)}. \tag{6}$$

During data collection, all parameters, including laser intensities, gain, and exposure time, were fixed. For each fluorophore-tagged ENaC subunit pair, k_1 and k_2 were determined from the slope of linear fits to X-eCFP versus Y-eYFP, and X-eYFP versus Y-eCFP scatter plots, respectively (see Figs. 4–6). The constant *C* of 0.32 ± 0.04 (458/480 and 488/535 nm) and 0.52 ± 0.03 (with 442/470 and 514/550 nm) for our system was experimentally determined for each fluorophore-tagged ENaC subunit combination and subsequently used to generate predicted FIR lines describing possible channel subunit relations and to scale data (refer to Fig. 1).

The FIR method assumes independent eCFP and eYFP emissions. However, these fluorophores when fused to ENaC form FRET pairs (Staruschenko et al., 2004a) resulting in artificially reduced and enhanced eCFP and eYFP emissions, respectively. When scaling with the constant *C* as done here, the reduction and increase in eCFP/eYFP emissions do not bias results when subunits are represented in the channel at equal levels (see Figs. 1 and 2); however, when one subunit is more prevalent than another, FRET leads to a modest error in FIR analysis where differences in subunit number are marginally exaggerated (see also Zheng and Zagotta, 2004). We calculate that errors of this nature lead to at most a 20% discrepancy when determining subunit relationships with the current emission and excitation settings (see Figs. 1 and 2).

Electrophysiology

Whole-cell macroscopic current recordings of hENaC expressed in CHO cells were made under voltage-clamp conditions using standard methods (Staruschenko et al., 2004a,b; Tong et al., 2004). Current through ENaC was the inward, amiloride-sensitive Na^+ current with a bath solution of (in mM)

160 NaCl, 1 $CaCl_2$, 2 $MgCl_2$, and 10 HEPES (pH 7.4) and a pipette solution of (in mM) 120 CsCl, 5 NaCl, 5 EGTA, 2 $MgCl_2$, 2 ATP, 0.1 GTP, 10 HEPES (pH 7.4). Current recordings were acquired with an Axopatch 200B (Axon Instruments, Union City, CA) interfaced via a Digidata 1322A (Axon Instruments) to a PC running the pClamp 9.2 suite of software (Axon Instruments). All currents were filtered at 1 kHz. Voltage ramps (300 ms) from a holding potential of from 40–60 mV to -100 mV were used to generate current-voltage (I-V) relations and to measure ENaC activity at -80 mV. Whole-cell capacitance was routinely compensated and was $\sim$9 pF. Series resistances, on average 2–5 MΩ, were also compensated.

Statistics

FIR data were fit with linear regression lines. All data reported as mean $\pm$ SE $P \leq 0.05$ were significant with data analyzed with the appropriate *t*-test.

RESULTS

Plasma membrane ENaC contains equal numbers of α-, β-, and γ-subunits

To determine the relative stoichiometry of α-, β-, and γ-subunits in heteromeric ENaC within the plasma membrane, we combined a fluorescence-based approach (FIR) to determine subunit relations with total internal reflection fluorescence microscopy to focus on signals from membrane channels. Fig. 1 shows fluorescence micrographs from control experiments validating this ratiometric approach for establishing relative membrane levels of proteins. Cells in Fig. 1 *A* were transfected with membrane localized eCFP-m and eYFP-m alone and together at ratios of 1:1, 2:1, 1:2, 3:1, and

1:3 with emissions from eCFP (*top*; *pseudocolored cyan*) and eYFP (*bottom*; *pseudocolored yellow*) quantified in TIRF after exciting with 442 and 514 nm, respectively. Quantifying emissions from eCFP-m and eYFP-m at expression ratios of 2:1 and 3:1, as well as making a similar measurement in parallel with expression ratios of 1:2 and 1:3, enabled determination of the scaling factor C, which accounts for differences in laser excitation intensities, extinction coefficients, quantum yields, and other fluorophore properties. Fig. 1 *B* shows the regression lines from data points plotted with eCFP (F_{eCFP}) versus eYFP (F_{eYFP}) fluorescence emissions from cells expressing eCFP-m and eYFP-m at 3:1 (*green*), 2:1 (*blue*), 1:1 (*red*), and 0:1 (*yellow*) ratios and their parallel complements. The fluorescence intensity ratios k_1 and k_2 for expression at 2:1 and 1:2 were 0.95 and 0.24, respectively, yielding a ratio of membrane eCFP-m to eYFP-m of 2.0. For expression at 3:1 and 1:3, k_1 and k_2 were 1.4 and 0.18, respectively, giving a ratio of 2.80. The constant C for these experiments was 0.52 ± 0.03. Fig. 1 *C* shows predicted (*black*) regression lines defining expected eCFP-m and eYFP-m levels in the membrane at each expression ratio, as well as experimental regression lines from Fig. 1 *B* scaled with the constant C. The slopes of the regression lines for ratios of 2:1 (k_1) and 1:2 (k_2) were 0.47 and 1.9, respectively, again yielding a membrane level of eCFP-m to eYFP-m of 2.0. For eCFP-m and eYFP-m at ratios of 3:1 and 1:3, k_1 and k_2 were 0.36 and 2.8, respectively, giving, as expected, a membrane level of eCFP-m to eYFP-m of 2.8. The unscaled and scaled FIR for expression at 1:1 were 0.58 and 1.1. Because C defines the relationship between eCFP and eYFP emissions under our experimental settings, the unscaled FIR for 1:1 expression should be very close to C. These results are consistent with this expectation.

The ratiometric approach used in this study assumes independent eCFP and eYFP emissions. However, these fluorophores in some instances, such as when they are fused to ENaC subunits (Staruschenko et al., 2004a), form FRET pairs resulting in artificially reduced and enhanced eCFP and eYFP emissions, respectively. When scaling with C, the

reduction/increase in eCFP/eYFP emissions do not bias results in a ratiometric analysis, as shown in Fig. 2, when subunits are represented in the channel at equal levels; however, when one subunit is more prevalent than another, FRET leads to a modest error in FIR analysis (see also Zheng and Zagotta, 2004). Fig. 2, *left*, shows experimentally determined unscaled FIR lines (*blue*) for eCFP-m and eYFP-m expressed at 2:1 and 1:2. Also shown are predicted FIR lines (*red*) for these fluorophores if they had formed a FRET pair, as they do when fused to ENaC subunits. To reiterate, in the absence of any FRET, k_1 and k_2 are 0.95 and 0.24, respectively. With 30% FRET, k_1' and k_2' would instead be 0.66 and 0.17. However, when scaled with C and C' as shown in Fig. 2, *right*, both conditions yield X/Y ratios of 2.0. By calculating FIR in the presence of FRET for fluorophores in a possible channel complex at unequal levels (we used 2:1), we established the maximum error introduced by FRET when determining X/Y ratios to be <20%. The green lines in Fig. 2, *right*, graphically display this error. The error introduced by FRET can also be visualized in Fig. 1 *B* by comparing the experimentally established FIR line for eCFP-m plus eYFP-m at a 1:1 ratio versus that for CGY-m, which is a fusion protein containing both fluorophores as an active FRET pair with a FRET of 20%, an efficiency greater than that between ENaC subunits (Staruschenko et al., 2004a). Thus, FRET between fluorophores in a channel complex has no effect on FIR measurements as established with these settings and scaling, or at most, only modestly affects X/Y ratios established with FIR.

For TIRF-FIR analysis of subunit relationships in ENaC, an eCFP-tagged channel subunit was coexpressed with a distinct eYFP-tagged subunit plus an untagged distinct third subunit (e.g., eCFP-α + eYFP-β + γ-ENaC). To define C, a similar measurement was made in parallel where the fluorescent tag was exchanged between the two labeled subunits (e.g., eCFP-α + eYFP-β + γ-ENaC). The fluorophore-tagged ENaC subunits used here, as reported previously, form functional channels indistinct from ENaC in native epithelia (Staruschenko et al., 2004a). Fig. 3 shows representative
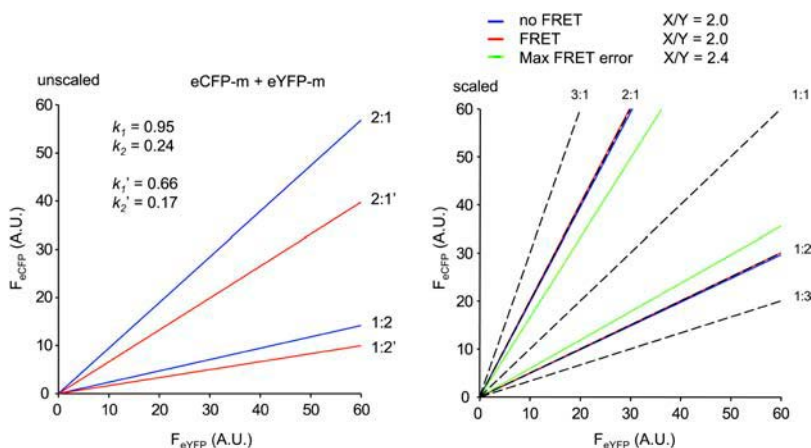

FIGURE 2 FRET has little impact on FIR. (*Left*) Unscaled best-fit linear regressions lines of data points for eCFP and eYFP emissions from cells expressing eCFP-m and eYFP-m at cDNA ratios of 2:1 and 1:2 in the absence of FRET (*blue*) and with hypothetical FRET of 30% between these fluorophores (*red*; 2:1' and 1:2'). Also shown are the FIR values k_1 and k_2, and k_1' and k_2' in the absence and presence of FRET, respectively. (*Right*) Results from panel *A* scaled using the constant C (*blue*) and C' (*red*). The green lines represent the maximum possible error introduced by FRET for the 2:1 and 1:2 regression lines. Black dashed lines indicated predicted eCFP-m and eYFP-m membrane levels at the indicated expression ratios.
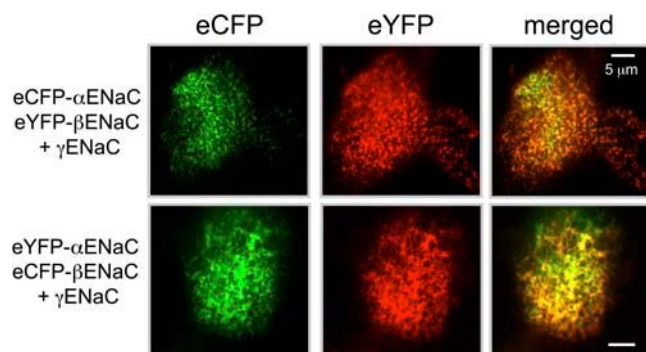
FIGURE 3 ENaC expressed in the membrane. Fluorescence micrographs of COS-7 cells coexpressing eCFP-αENaC + eYFP-βENaC and untagged γENaC (*top row*), and eCFP-βENaC + eYFP-αENaC and untagged γENaC (*bottom row*) collected with total internal reflection fluorescence microscopy. Fluorescence emissions from eCFP- (*pseudocolored green*) and eYFP- (*pseudocolored red*) tagged ENaC within the plasma membrane are shown in the left and middle columns. The right column shows merged images.

fluorescence images collected with TIRF microscopy from cells overexpressing eCFP-α + eYFP-β + γENaC and its complement of eYFP-α + eCFP-β + γENaC. For these images, eCFP emissions are pseudocolored green and shown in the first column and eYFP emissions are pseudocolored red and shown in the middle column. The last column contains merged images showing colocalization of the eCFP- and eYFP-tagged ENaC subunits within the membrane.

Because eCFP and eYFP are genetically linked to channel subunits, emissions from the respective fluorophores are directly proportional to the number of eCFP- and eYFP-tagged subunits in the membrane. The slope of the linear fits to the eCFP versus eYFP scatter plots for each tagged-subunit pair (k_1; see Materials and Methods and Figs. 4–6) and its complementary pair (k_2) describe the relationship between the

differentially fluorophore-tagged subunits within the membrane. The relative ratio of subunits at the surface membrane, then, is calculated using k_1 and k_2 (see Materials and Methods).

Fig. 4 shows scatter plots and associated linear fits (*red lines*) of F_{eCFP} versus F_{eYFP} intensities from cells expressing eCFP-α + eYFP-β + γENaC (*A*) and eYFP-α + eCFP-β + γENaC (*C*). Plots were created from cells with a range of fluorescence intensities and, thus, subunit expression levels. Predicted relative (α to β) stoichiometry FIR lines calculated using *C* (see Materials and Methods) are shown as dashed black lines. For each pair of tagged-ENaC subunits, we also titrated expression of the eCFP-tagged subunit such that it was equal to, twice as much, and threefold that of the eYFP-tagged subunit. Data points (*circles*) from cells transfect with equal levels of eCFP-tagged and eYFP-tagged subunit cDNA are red, those with twice as much eCFP-tagged subunit cDNA are blue, and those with threefold are green. Fig. 4, *B* and *D*, show the fluorescence intensity ratios for eCFP-α + eYFP-β + γENaC and its complementary pair, respectively, as a function of eCFP-tagged-subunit titration. From Fig. 4, *A* and *C*, k_1 and k_2 were 1.19 ($r^2 = 0.75$) and 0.84 ($r^2 = 0.68$), respectively, yielding an α/β subunit ratio of 1.19 suggesting that there are equal numbers of each subunit in the plasma membrane. We argue that these subunits are contained within fully oligomerized ENaC within the plasma membrane for when the expression level of the eCFP-tagged subunit was increased, even to threefold of that of the eYFP-tagged subunit, fluorescence intensities ratios describing the relationship of α- to βENaC remained unchanged demonstrating that the fluorescence intensities of fluorophore-tagged α- and βENaC in the membrane are directly coupled. These titration experiments also suggest that the channel has a fixed stoichiometry at steady state with this stoichiometry and not the greater availability of the eCFP-
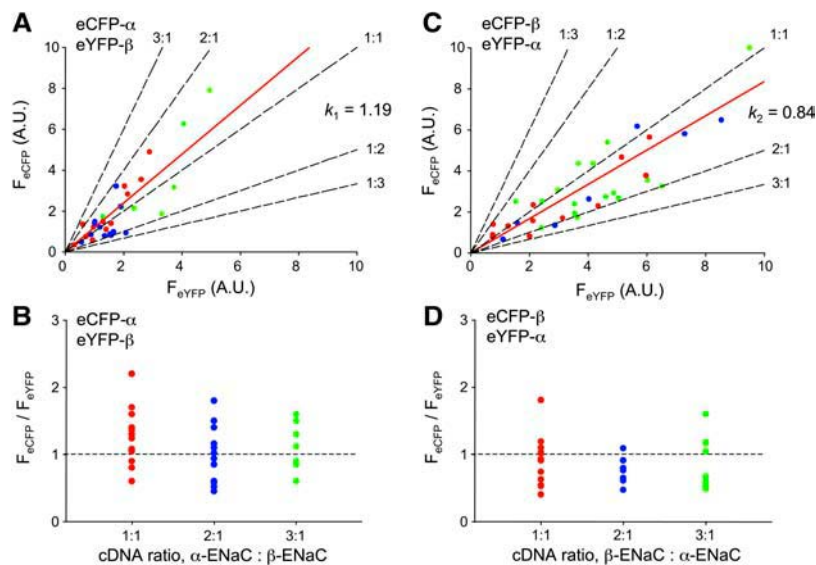

FIGURE 4 The relative amounts of α- and β-subunits in membrane ENaC are the same. Scatter plot of eCFP versus eYFP fluorescence emissions collected with TIRF microscopy from cells coexpressing eCFP-αENaC + eYFP-βENaC and untagged γENaC (*A*) and eCFP-βENaC + eYFP-αENaC and untagged γENaC (*C*). Solid red lines are the best-fit linear regression lines (m = fluorescence intensity ratio for panels *A* and *C*, which are k_1 and k_2); black dashed lines predict subunit relations at the indicated stoichiometry; red, blue, and green circles represent data points from cells transfected with equal amounts of eCFP- and eYFP-tagged subunit and those with twice and three times as much eCFP- versus eYFP-tagged subunit, respectively. Scatter plots of the quotient of eCFP/eYFP fluorescence emissions from panel *A* (*B*) and panel *C* (*D*) as a function of the relative eCFP- to eYFP-tagged subunit expression level.

tagged subunit determining FIR. Moreover, these results suggest that when all three ENaC subunits are coexpressed, heteromeric channels are formed preferentially over homomeric channels.

Fig. 5, *A* and *C*, show scatter plots, associated linear fits, and predicted FIR lines for cells expressing eCFP-β + eYFP-γ + αENaC (*A*) and eYFP-β + eCFP-γ + αENaC, respectively. Similar to Fig. 4, the eCFP-tagged subunit cDNA level was titrated with red circles representing cells transfected with equivalent eCFP- and eYFP-tagged subunit cDNA levels, blue with twice as much eCFP-tagged subunit, and green thrice as much. Fig. 5, *B* and *D*, show the fluorescence intensity ratios for eCFP-β + eYFP-γ + αENaC and its complementary pair, respectively, as a function of eCFP-tagged-subunit titration. From Fig 5, *A* and *C*, k_1 and k_2 were 0.98 ($r^2 = 0.86$) and 1.02 ($r^2 = 0.88$), respectively, yielding a β/γ subunit ratio of 0.98 suggesting that there are equal numbers of each subunit in the plasma membrane. Again, we believe these subunits were contained within fully oligomerized ENaC within the plasma membrane for titration of the eCFP-tagged subunit had little effect on FIR describing the relationship of β- to γENaC.

Fig. 6, *A* and *C*, show scatter plots, associated linear fits, and predicted FIR lines for cells expressing eCFP-α + eYFP-γ + βENaC (*A*) and eYFP-α + eCFP-γ + βENaC, respectively. Similar to Figs. 4 and 5, the eCFP-tagged subunit cDNA level was titrated with red circles representing cells transfected with equivalent eCFP- and eYFP-tagged subunit cDNA levels, blue with twice as much eCFP-tagged subunit, and green thrice as much. Fig. 6, *B* and *D*, show the fluorescence intensity ratios for eCFP-α + eYFP-γ + βENaC and its complementary pair, respectively, as a function of eCFP-tagged-subunit titration. From Fig. 6, *A* and *C*, k_1 and k_2 were 1.02 ($r^2 = 0.81$) and 0.96 ($r^2 = 0.86$), re-

spectively, yielding an α/γ subunit ratio of 1.03 suggesting that there are equal numbers of each subunit in the plasma membrane. Thus, the FIR results in Figs. 4–6 are consistent with a relative subunit stoichiometry of 1α:1β:1γ.

Fig. 7 shows the fluorescence intensity ratio with wide-field (epifluorescence) imaging for the cells expressing eCFP-α + eYFP-γ + βENaC (*circles*) and eCFP-γ + eYFP-α + βENaC (*squares*) imaged with TIRF microscopy in Fig. 6. As expected, but in contrast to the TIRF-FIR results in Fig. 6, the ratio in wide field showed a clear dependence on titration of the eCFP-tagged subunit cDNA. A comparison of the results in Figs. 6 and 7 supports the idea that in our TIRF-FIR experiments, ENaC subunits arrived at the membrane together preferring a heteromeric channel complex with a fixed stoichiometry. Moreover, they are consistent with channel stoichiometry defining subunit (fluorescence) relations, as compared to random distribution of subunits within the membrane.

Functional ENaC contains equal numbers of α-, β-, and γ-subunits

To complement TIRF-FIR experiments, we also tested ENaC subunit stoichiometry with electrophysiology to assess subunit relations in the functional channel. Fig. 8 shows typical current traces (*A*) and a summary graph (*B*) of findings from a subunit-dose experiment where macroscopic amiloride-sensitive ENaC currents were quantified in CHO cells transfected with α-, β-, and γ-ENaC with subunit cDNA levels either all being equal at 0.6 and 0.2 μg each per 35 mm^2, or with α but not β and γ being expressed at the higher dose, or with β and γ but not α being expressed at the higher dose. Our rationale is that if the channel complex contains each subunit at the same relative ratio and
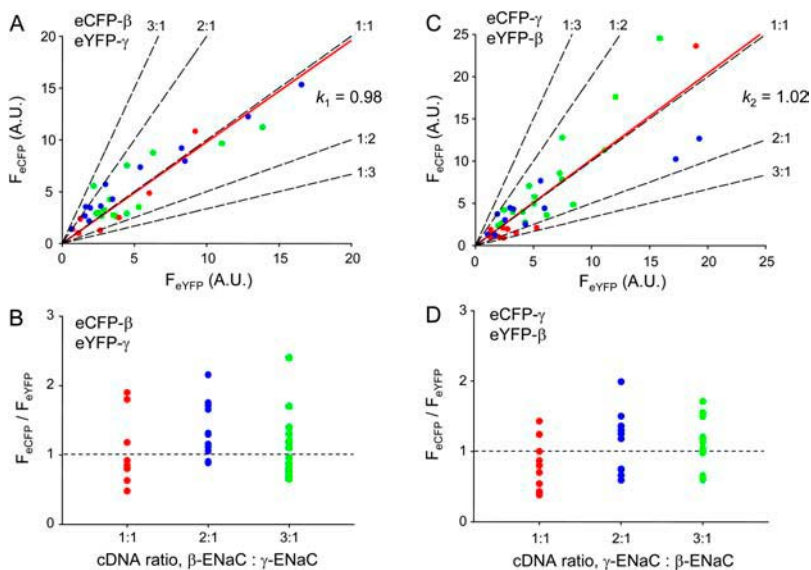

FIGURE 5 The relative amounts of β- and γ-subunits in membrane ENaC are the same. Scatter plot of eCFP versus eYFP fluorescence emissions collected with TIRF microscopy from cells coexpressing eCFP-βENaC + eYFP-γENaC and untagged αENaC (*A*) and eCFP-γENaC + eYFP-βENaC and untagged αENaC (*C*). Solid red lines are the best-fit linear regression lines (*m* = fluorescence intensity ratio for panels A and C, which are k_1 and k_2); black dashed lines predict subunit relations at the indicated stoichiometry; red, blue, and green circles represent data points from cells transfected with equal amounts of eCFP- and eYFP-tagged subunit and those with twice and three times as much eCFP- versus eYFP-tagged subunit, respectively. Scatter plots of the quotient of eCFP/eYFP fluorescence emissions from panel *A* (*B*) and panel *C* (*D*) as a function of the relative eCFP- to eYFP-tagged subunit expression level.
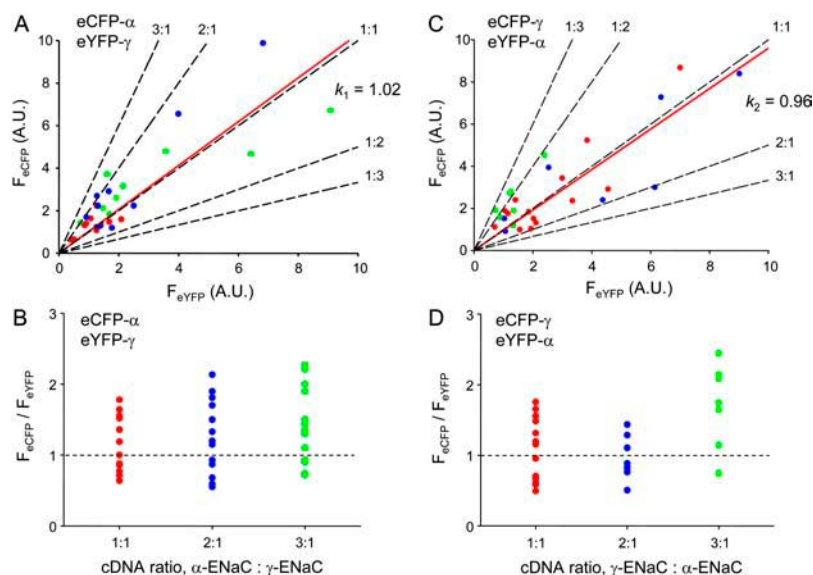
FIGURE 6   The relative amounts of α- and γ-subunits in membrane ENaC are the same. Scatter plot of eCFP versus eYFP fluorescence emissions collected with TIRF microscopy from cells coexpressing eCFP-αENaC + eYFP-γENaC and untagged βENaC (*A*) and eCFP-γENaC + eYFP-αENaC and untagged βENaC (*C*). Solid red lines are the best-fit linear regression lines (m = fluorescence intensity ratio for panels *A* and *C*, which are k_1 and k_2); black dashed lines predict subunit relations at the indicated stoichiometry; red, blue, and green circles represent data points from cells transfected with equal amounts of eCFP- and eYFP-tagged subunit and those with twice and three times as much eCFP- versus eYFP-tagged subunit, respectively. Scatter plots of the quotient of eCFP/eYFP fluorescence emissions from panel *A* (*B*) and panel *C* (*D*) as a function of the relative eCFP- to eYFP-tagged subunit expression level.

heteromeric channels are preferentially formed, then increasing the expression of one subunit compared to that of the others should have little effect on activity; however, in contrast, if there are more αENaC subunits in the final channel complex, then titration of this subunit so that it is at triple the level of the other two subunits should be equivalent to simply increasing expression of all three subunits in unison threefold. The results in Fig. 8 clearly show that only equivalent increases in subunit cDNA levels of all three subunits result in increases in ENaC activity. Such a finding is consistent with each subunit being in the channel at similar levels and not with the notion that one subunit is more prevalent in the final channel complex.

ENaC has a limiting stoichiometry of 1α:1β:1γ

If ENaC is a heteromeric channel having a relative, limiting subunit stoichiometry of 1:1:1, as results in Figs. 3–8
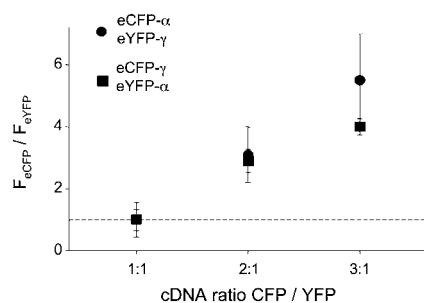

FIGURE 7   Increasing expression eCFP-tagged ENaC subunits increases total cellular eCFP fluorescence emissions. Summary graph of the quotient of eCFP/eYFP fluorescence emissions as a function of the relative eCFP- to eYFP-tagged subunit expression level collected with wide-field epifluorescence microscopy from the cells in Fig. 6 coexpressing eCFP-αENaC + eYFP-γENaC and untagged βENaC (●) and eCFP-γENaC + eYFP-αENaC and untagged βENaC (■).

suggest, then expressing α-eCFP + β-eYFP + γ-eYFP and its complement should yield an α to β + γ relationship of 0.5. Fig. 9 shows results from experiments testing this idea. Fig. 9, *A–C*, contains data points and associated linear fits and resulting k_1 and k_2 for α-eCFP + β-eYFP + γ-eYFP (*red*) and α-eYFP + β-eCFP + γ-eCFP (*blue*); β-eCFP + α-eYFP + γ-eYFP (*red*) and β-eYFP + α-eCFP + γ-eCFP (*blue*); and γ-eCFP + α-eYFP + β-eYFP (*red*) and γ-eYFP + α-eCFP + β-eCFP (*blue*). For these experiments, cells were transfected with 0.2 μg cDNA for each subunit. For all combinations where the X-subunit was fused to a fluorescent tag and the other two distinct (Y-) subunits to the alternative fluorescent tag, the calculated relations for X to Y were 0.5 suggesting that for every X-subunit there were two Y-subunits in the channel. These results are consistent with the limiting stoichiometry of 1α:1β:1γ.

DISCUSSION

Determining quaternary structure (e.g., subunit stoichiometry) is critical to understanding channel regulation at the cellular and molecular levels. Unfortunately, investigation of subunit stoichiometry for most heteromeric channel complexes has proven extremely challenging. Although the atomic resolution of several bacterial ion channels has provided rich information about their molecular architecture (Doyle et al., 1998; MacKinnon, 2003, 2004; Zhou et al., 2001), it has been difficult to universally apply this strategy to all integral membrane proteins, particularly heteromeric mammalian ion channels. As yet, the epithelial Na$^+$ channel falls into the category of channels for which atomic level resolution has not been established. Several laboratories, however, have provided important information about subunit relations within ENaC. Two competing subunit stoichiometries, often arrived at using similar experimental approaches,
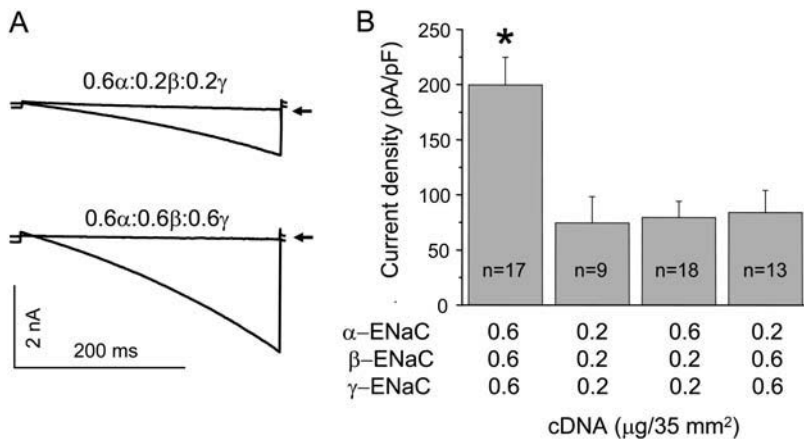
FIGURE 8 ENaC has a relative subunit stoichiometry of $1\alpha{:}1\beta{:}1\gamma$. (*A*) Overlays of typical macroscopic Na$^+$ currents in CHO cells transfected with 0.6, 0.2, and 0.2 μg (*top*), and 0.6, 0.6, and 0.6 μg (*bottom*) of α-, β-, and γENaC before and after amiloride (noted by *arrow*). Currents elicited by voltage ramping from 60 to -100 mV. (*B*) Summary graph of ENaC activity (amiloride-sensitive current density at -80 mV) in CHO cells transfected with α-, β-, and γENaC cDNAs at the noted concentrations. The asterisk (*) is versus all other groups.

have been proposed for this channel: ENaC is believed to be either a heterotetramer containing $2\alpha{:}1\beta{:}1\gamma$ (Firsov et al., 1998; Kosari et al., 1998) or a channel with a higher order structure possibly containing $3\alpha{:}3\beta{:}3\gamma$ (Snyder et al., 1998; Eskandari et al., 1999). In this study, we used a novel biophysical approach to increase understanding of the subunit relationship within membrane ENaC. Our results are most consistent with membrane ENaC containing equal numbers of each of its three component subunits.

To place these findings in the context of that reported previously by others, our results appear to be most supportive of a higher order channel structure compared to a heterotetrameric structure. We argue this point from the current TIRF-FIR results demonstrating that each ENaC subunit is in the plasma membrane at the same relative ratio and that increasing the expression of one subunit does not change this ratio suggesting that channel stoichiometry and subunit relations within the oligomerized channel define the membrane levels of each subunit. Importantly, probing the subunit relations within functional channels using a simple but direct electrophysiology approach was also consistent with a limiting stoichiometry for ENaC of $1\alpha{:}1\beta{:}1\gamma$. Moreover, when one type of ENaC subunit was distinguished fluorescently (i.e., tagged with eCFP) from the other two, which were treated equally (i.e., both tagged with eYFP), the relative membrane levels of the distinguished subunit compared to the combination of the other two was 1:2, which is consistent with a limiting stoichiometry of 1:1:1.

It is hard to reconcile why ENaC appears to have a tetrameric structure in some studies and a higher order structure in others. One possible explanation recently suggested by Hughey and colleagues (Hughey et al., 2004) is that distinct forms of heteromeric ENaC, containing each of the three types of subunits, reach the membrane. Although the functional ramifications and importance of these possibly distinct forms of ENaC remain to be fully determined, it is
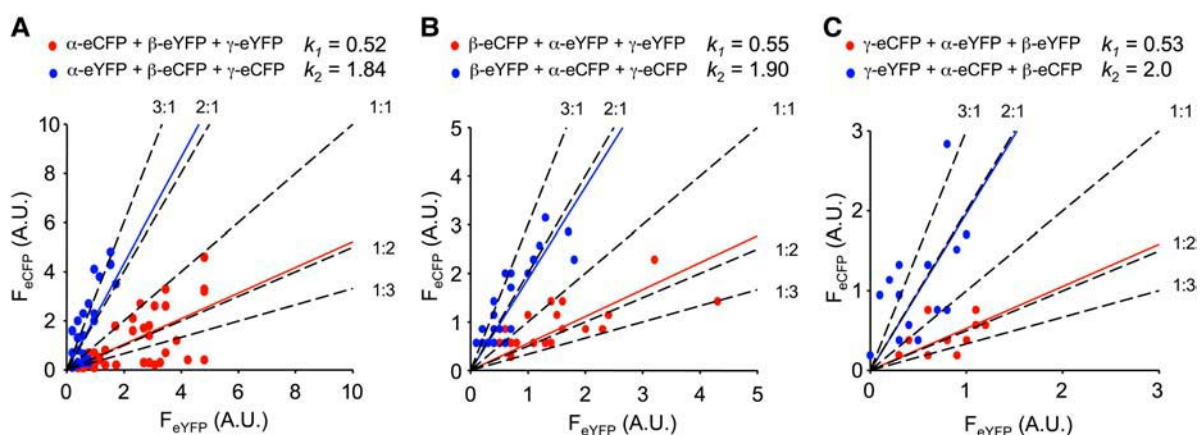

FIGURE 9 ENaC has a limiting stoichiometry of $1\alpha{:}1\beta{:}1\gamma$. Scatter plots of eCFP versus eYFP fluorescence emissions collected with TIRF microscopy from cells coexpressing (*A*) eCFP-αENaC + eYFP-βENaC + eYFP-γENaC (*red circles*) and eYFP-αENaC + eCFP-βENaC + eCFP-γENaC (*blue circles*); (*B*) eCFP-βENaC + eYFP-αENaC + eYFP-γENaC (*red circles*) and eYFP-βENaC + eCFP-αENaC + eCFP-γENaC (*blue circles*); and (*C*) eCFP-γENaC + eYFP-αENaC + eYFP-βENaC (*red circles*) and eYFP-γENaC + eCFP-αENaC + eCFP-βENaC (*blue circles*). Solid red (k_1) and blue (k_2) lines are the best-fit linear regression lines and black dashed lines predict subunit relations at the indicated stoichiometry. For all experiments, ENaC subunit cDNAs were expressed at 0.2 μg each.

conceivable that they have different stoichiometries. If this is indeed the case, then COS-7 and CHO cells, as used in this study, must have preferentially expressed only one possible type of ENaC. It is important to realize that distinct forms of ENaC within the membrane may reflect leak in an over-expression system. Thus, we as well as others investigating ENaC stoichiometry in heterologous systems have to consider that probing subunit relationships is likely impacted by the expression system used particularly when considering quality control check points determining fidelity of subunit folding, oligomerization, and transit to the membrane. The current studies were performed in a mammalian expression system, whereas, the initial studies probing ENaC subunit stoichiometry were performed in the amphibian *Xenopus laevis* oocyte expression system (Kosari et al., 1998; Firsov et al., 1998; Eskandari et al., 1999). This may contribute to apparent inconsistencies. It is, currently, unclear how best to probe stoichiometry of endogenous ENaC expressed within native epithelia and, thus, it becomes important to probe subunit relations in as many different systems as possible.

Parallels with the fourfold internal symmetry model established for K^+ channels comprised of subunits having only two transmembrane domains, such as KcsA (MacKinnon, 2003) and inward-rectifier K_{ir} channels (Yang et al., 1995), lends great appeal to the $2\alpha{:}1\beta{:}1\gamma$ stoichiometry model for ENaC. But important differences between these channels must be recognized, primary of which is that the pore of K_{ir} and KcsA is encircled by four usually identical subunits (MacKinnon, 2003), which is different from ENaC. Each of the three distinct types of ENaC subunits contribute to formation of the pore (Firsov et al., 1998; Canessa et al., 1994). When heteromeric K_{ir} do form, they contain at most only two distinct types of pore-forming subunits (Kofuji et al., 1995; Krapivinsky et al., 1995; Corey et al., 1998).

The cation P2X channels also contain only two trans-membrane domains, and compared to K_{ir} and KcsA, have considerably more tertiary structure in common with ENaC/Deg, including a large cysteine-rich extracellular domain (North, 1996; Benos and Stanton, 1999; Kellenberger and Schild, 2002; Newbolt et al., 1998; Khakh et al., 2001). Such a large ectodomain is rather unique for ion channels found only in ENaC/Deg and P2X receptors. The subunit stoichiometry for P2X channels is currently thought to be trimeric or a multiple of trimers (North, 1996; Nicke et al., 1998, 2003; Stoop et al., 1999; Robertson et al., 2001). The current results are consistent with ENaC having a similar quaternary structure. The trimeric structure of P2X suggests that the stoichiometry of a channel containing subunits with only two transmembrane domains is not constrained by a tetrameric model.

In addition to determining ENaC subunit relations, the current results provide information about the preference for ENaC subunits to form heteromeric channels over homomeric channels. The current electrophysiology experiments testing

subunit titration clearly indicate, at the functional level, that when all three subunits are available for oligomerization, formation of heteromeric channels containing each of the three subunits is favored over that of homomeric channels. This finding is consistent with many other studies investigating ENaC function (Canessa et al., 1994; Firsov et al., 1998; Fyfe and Canessa, 1998). However, if homomeric channels have greatly decreased activity, which they appear to (Canessa et al., 1994; Fyfe and Canessa, 1998; Canessa et al., 1993), then the significance with respect to stoichiometry of such findings is lessened for contribution to activity by homomeric channels must be overwhelmed by more active heteromeric channels. The current TIRF-FIR results demonstrate that when all three subunits are coexpressed, increased expression of one subunit does not promote the appearance of homomeric channels in the membrane. Importantly, the current TIRF-FIR approach was not limited by a possible decrease in activity of homomeric channels complicating interpretation and thus, makes a strong argument that heteromeric ENaC is preferentially formed over homomeric channels when all three subunits are available for oligomerization. The ramifications of this finding are clear for tissues, such as the distal renal nephron, that coexpress each of the three ENaC subunits. It suggests that inadequate expression of one subunit would limit ENaC activity. This prediction is entirely consistent with findings from engineered mice with the salt wasting disease pseudohypoaldosteronism where the genes encoding either α-, β-, or γ-ENaC had been disrupted (reviewed by Hummler and Horisberger, 1999; Snyder, 2002). Similarly, decreased expression of any of the three human ENaC subunits leads to pseudohypoaldosteronsim due to loss of ENaC function (Thomas et al., 2002; Saxena et al., 2002; Adachi et al., 2001).

REFERENCES

Adachi, M., K. Tachibana, Y. Asakura, S. Abe, J. Nakae, T. Tajima, and K. Fujieda. 2001. Compound heterozygous mutations in the gamma subunit gene of ENaC (1627delG and 1570–1G→A) in one sporadic Japanese patient with a systemic form of pseudohypoaldosteronism type 1. *J. Clin. Endocrinol. Metab.* 86:9–12.

Benos, D. J., and B. A. Stanton. 1999. Functional domains within the degenerin/epithelial sodium channel (Deg/ENaC) superfamily of ion channels. *J. Physiol. (Lond.).* 520:631–644.

Canessa, C. M., J. D. Horisberger, and B. C. Rossier. 1993. Epithelial sodium channel related to proteins involved in neurodegeneration. *Nature.* 361:467–470.

Canessa, C. M., L. Schild, G. Buell, B. Thorens, I. Gautschi, J. D. Horisberger, and B. C. Rossier. 1994. Amiloride-sensitive epithelial Na channel is made of three homologous subunits. *Nature*. 367:463–467.

Corey, S., G. Krapivinsky, L. Krapivinsky, and D. E. Clapham. 1998. Number and stoichiometry of subunits in the native atrial G-protein-gated K+ channel, IKACh. *J. Biol. Chem*. 273:5271–5278.

Doyle, D. A., C. J. Morais, R. A. Pfuetzner, A. Kuo, J. M. Gulbis, S. L. Cohen, B. T. Chait, and R. MacKinnon. 1998. The structure of the potassium channel: molecular basis of K+ conduction and selectivity. *Science*. 280:69–77.

Eskandari, S., P. M. Snyder, M. Kreman, G. A. Zampighi, M. J. Welsh, and E. M. Wright. 1999. Number of subunits comprising the epithelial sodium channel. *J. Biol. Chem*. 274:27281–27286.

Firsov, D., I. Gautschi, A. M. Merillat, B. C. Rossier, and L. Schild. 1998. The heterotetrameric architecture of the epithelial sodium channel (ENaC). *EMBO J*. 17:344–352.

Fyfe, G. K., and C. M. Canessa. 1998. Subunit composition determines the single channel kinetics of the epithelial sodium channel. *J. Gen. Physiol*. 112:423–432.

Hughey, R. P., J. B. Bruns, C. L. Kinlough, and T. R. Kleyman. 2004. Distinct pools of epithelial sodium channels are expressed at the plasma membrane. *J. Biol. Chem*. 279:48491–48494.

Hummler, E., and J. D. Horisberger. 1999. Genetic disorders of membrane transport. V. The epithelial sodium channel and its implication in human diseases. *Am. J. Physiol*. 276:G567–G571.

Kellenberger, S., and L. Schild. 2002. Epithelial sodium channel/degenerin family of ion channels: a variety of functions for a shared structure. *Physiol. Rev*. 82:735–767.

Khakh, B. S., G. Burnstock, C. Kennedy, B. F. King, R. A. North, P. Seguela, M. Voigt, and P. P. Humphrey. 2001. International union of pharmacology. XXIV. Current status of the nomenclature and properties of P2X receptors and their subunits. *Pharmacol. Rev*. 53:107–118.

Kofuji, P., N. Davidson, and H. A. Lester. 1995. Evidence that neuronal G-protein-gated inwardly rectifying K+ channels are activated by G beta gamma subunits and function as heteromultimers. *Proc. Natl. Acad. Sci. USA*. 92:6542–6546.

Kosari, F., S. Sheng, J. Li, D. O. Mak, J. K. Foskett, and T. R. Kleyman. 1998. Subunit stoichiometry of the epithelial sodium channel. *J. Biol. Chem*. 273:13469–13474.

Krapivinsky, G., E. A. Gordon, K. Wickman, B. Velimirovic, L. Krapivinsky, and D. E. Clapham. 1995. The G-protein-gated atrial K+ channel IKACh is a heteromultimer of two inwardly rectifying K(+)-channel proteins. *Nature*. 374:135–141.

Lifton, R. P., A. G. Gharavi, and D. S. Geller. 2001. Molecular mechanisms of human hypertension. *Cell*. 104:545–556.

MacKinnon, R. 2003. Potassium channels. *FEBS Lett*. 555:62–65.

MacKinnon, R. 2004. Potassium channels and the atomic basis of selective ion conduction (Nobel Lecture). *Angew. Chem. Int. Ed. Engl*. 43:4265–4277.

Mall, M., B. Grubb, J. Harkema, W. O'Neal, and R. Boucher. 2004. Increased airway epithelial Na(+) absorption produces cystic fibrosis-like lung disease in mice. *Nat. Med*. 10:487–493.

McNicholas, C. M., and C. M. Canessa. 1997. Diversity of channels generated by different combinations of epithelial sodium channel subunits. *J. Gen. Physiol*. 109:681–692.

Newbolt, A., R. Stoop, C. Virginio, A. Surprenant, R. A. North, G. Buell, and F. Rassendren. 1998. Membrane topology of an ATP-gated ion channel (P2X receptor). *J. Biol. Chem*. 273:15177–15182.

Nicke, A., H. G. Baumert, J. Rettinger, A. Eichele, G. Lambrecht, E. Mutschler, and G. Schmalzing. 1998. P2X1 and P2X3 receptors form stable trimers: a novel structural motif of ligand-gated ion channels. *EMBO J*. 17:3016–3028.

Nicke, A., J. Rettinger, and G. Schmalzing. 2003. Monomeric and dimeric byproducts are the principal functional elements of higher order P2X1 concatamers. *Mol. Pharmacol*. 63:243–252.

North, R. A. 1996. Families of ion channels with two hydrophobic segments. *Curr. Opin. Cell Biol*. 8:474–483.

Robertson, S. J., S. J. Ennion, R. J. Evans, and F. A. Edwards. 2001. Synaptic P2X receptors. *Curr. Opin. Neurobiol*. 11:378–386.

Rohatgi, R., A. Greenberg, G. Burrow, P. Wilson, and L. Satlin. 2003. Na transport in autosomal recessive polycystic kidney disease (ARPKD) cyst lining epithelial cells. *J. Am. Soc. Nephrol*. 14:827–836.

Saxena, A., I. Hanukoglu, D. Saxena, R. J. Thompson, R. M. Gardiner, and A. Hanukoglu. 2002. Novel mutations responsible for autosomal recessive multisystem pseudohypoaldosteronism and sequence variants in epithelial sodium channel alpha-, beta-, and gamma-subunit genes. *J. Clin. Endocrinol. Metab*. 87:3344–3350.

Snyder, P. M. 2002. The epithelial Na(+) channel: cell surface insertion and retrieval in Na(+) homeostasis and hypertension. *Endocr. Rev*. 23:258–275.

Snyder, P. M., C. Cheng, L. S. Prince, J. C. Rogers, and M. J. Welsh. 1998. Electrophysiological and biochemical evidence that DEG/ENaC cation channels are composed of nine subunits. *J. Biol. Chem*. 273:681–684.

Staruschenko, A., J. L. Medina, P. Patel, M. S. Shapiro, R. E. Booth, and J. D. Stockand. 2004a. Fluorescence resonance energy transfer analysis of subunit stoichiometry of the epithelial Na+ channel. *J. Biol. Chem*. 279:27729–27734.

Staruschenko, A., A. Nichols, J. L. Medina, P. Camacho, N. N. Zheleznova, and J. D. Stockand. 2004b. Rho small GTPases activate the epithelial Na+ channel. *J. Biol. Chem*. 279:49989–49994.

Staruschenko, A., P. Patel, Q. Tong, J. L. Medina, and J. D. Stockand. 2004c. Ras activates the epithelial Na(+) channel through phosphoinositide 3-OH kinase signaling. *J. Biol. Chem*. 279:37771–37778.

Steyer, J. A., and W. Almers. 2001. A real-time view of life within 100 nm of the plasma membrane. *Nat. Rev. Mol. Cell Biol*. 2:268–275.

Stoop, R., S. Thomas, F. Rassendren, E. Kawashima, G. Buell, A. Surprenant, and R. A. North. 1999. Contribution of individual subunits to the multimeric P2X(2) receptor: estimates based on methanethiosulfonate block at T336C. *Mol. Pharmacol*. 56:973–981.

Taraska, J. W., D. Perrais, M. Ohara-Imaizumi, S. Nagamatsu, and W. Almers. 2003. Secretory granules are recaptured largely intact after stimulated exocytosis in cultured endocrine cells. *Proc. Natl. Acad. Sci. USA*. 100:2070–2075.

Thomas, C. P., J. Zhou, K. Z. Liu, V. E. Mick, E. MacLaughlin, and M. Knowles. 2002. Systemic pseudohypoaldosteronism from deletion of the promoter region of the human beta epithelial Na(+) channel subunit. *Am. J. Respir. Cell Mol. Biol*. 27:314–319.

Tong, Q., N. Gamper, J. L. Medina, M. S. Shapiro, and J. D. Stockand. 2004. Direct activation of the epithelial Na(+) channel by phosphatidylinositol 3,4,5-trisphosphate and phosphatidylinositol 3,4-bisphosphate produced by phosphoinositide 3-OH kinase. *J. Biol. Chem*. 279:22654–22663.

Veizis, E., C. Carlin, and C. Cotton. 2004. Decreased amiloride-sensitive Na+ absorption in collecting duct principal cells isolated from BPK ARPKD mice. *Am. J. Physiol*. 286:F244–F254.

Yang, J., Y. N. Jan, and L. Y. Jan. 1995. Determination of the subunit stoichiometry of an inwardly rectifying potassium channel. *Neuron*. 15:1441–1447.

Zheng, J., and W. N. Zagotta. 2004. Stoichiometry and assembly of olfactory cyclic nucleotide-gated channels. *Neuron*. 42:411–421.

Zhou, Y., J. H. Morais-Cabral, A. Kaufman, and R. MacKinnon. 2001. Chemistry of ion coordination and hydration revealed by a K+ channel-Fab complex at 2.0 A resolution. *Nature*. 414:43–48.